UNIVERSITY
OF OSLO

**Master's thesis**

# -sometitle-

Classifying N-body simulations with and without relativistic corrections
using machine learning techniques

**Johan Mylius Kroken**

Computational Science: Astrophysics
60 ECTS study points

Institute of Theoretical Astrophysics
Faculty of Mathematics and Natural Sciences


Autumn 2023

**Johan Mylius Kroken**

# -sometitle-

Classifying N-body simulations with and without relativistic corrections using machine learning techniques

Supervisors:
A David Fonseca Mota
B Julian Adamek
C Francisco Antonio Villaescusa Navarro

**Abstract**

On large scales, comparable to the horizon, relativistic effects will affect the cosmological observables. In order to solve for these effects, one need to consistently solve for the metric, velocities and densities in a particular gauge. When simulating large-scale structures we use N-body simulations, which are usually performed in the Newtonian limit. However, it is not obvious that Newtonian gravity yield a good global description of an inhomogeneous cosmology across all scales (Jeong, Fabian Schmidt and Hirata 2012). However, literature suggest that Newtonian simulations are still solving the dynamics correctly, even on large scales close to the horizon where relativistic effects are important but may be corrected for (Chisari and Zaldarriaga 2011) (Green and Wald 2012).

Recently, Adamek et al. 2016 developed a relativistic N-body code, `gevolution`, which evolves large scales structures based on the weak field expansion in GR. I investigate the differences in the gravitational dynamics between structures evolved with and without relativistic effects, with focus on the gravitational potential $\Phi$. This is a good choice for comparison as $\Phi$ is gauge invariant and the Newtonian and relativistic simulations are performed in different gauges.

The investigation is done by running 2000 simulations using identical $\Lambda$CDM cosmologies for the two gravity theories. The simulations are run using $64^4$ particles on a $256^3$ grid each with dimension 5120 Mpc/h which is a compromise in order to include both large and nonlinear scales. The data analysis consist of a preliminary analysis using conventional summary statistics, with focus on the bispectrum of $\Phi$. There is a difference in the two cases for low redshifts in the equilateral and squeezed configurations. However, the main idea is to train a Convolutional Neural Network (CNN) to classify the two cases, given snapshots of $\Phi$. The main analysis then involves interpretability of the CNN, which may be done by considering for instance saliency maps (Alqaraawi et al. 2020) or Grad-CAM (Selvaraju et al. 2020). In either case, revealing the features separating the two cases may help us understand the differences in the gravitational dynamics between the two theories. I expect that such a network is able to find relativistic corrections to the Newtonian snapshots that are of higher order than those obtained from power spectra and bispectra analysis. Further, it may also reveal which configurations of Fourier modes $\mathbf{k}$ yield the highest bispectral power, which for now is mainly trial and error.

# Contents

# List of Figures

# List of Tables

# Preface

Here comes your preface, including acknowledgments and thanks.

# Chapter 1

# Introduction

This is the introduction that will shortly be written. How fast does things change.

## 1.1 Motivation

## 1.2 Outline

## 1.3 Aim

## 1.4 Nomenclature

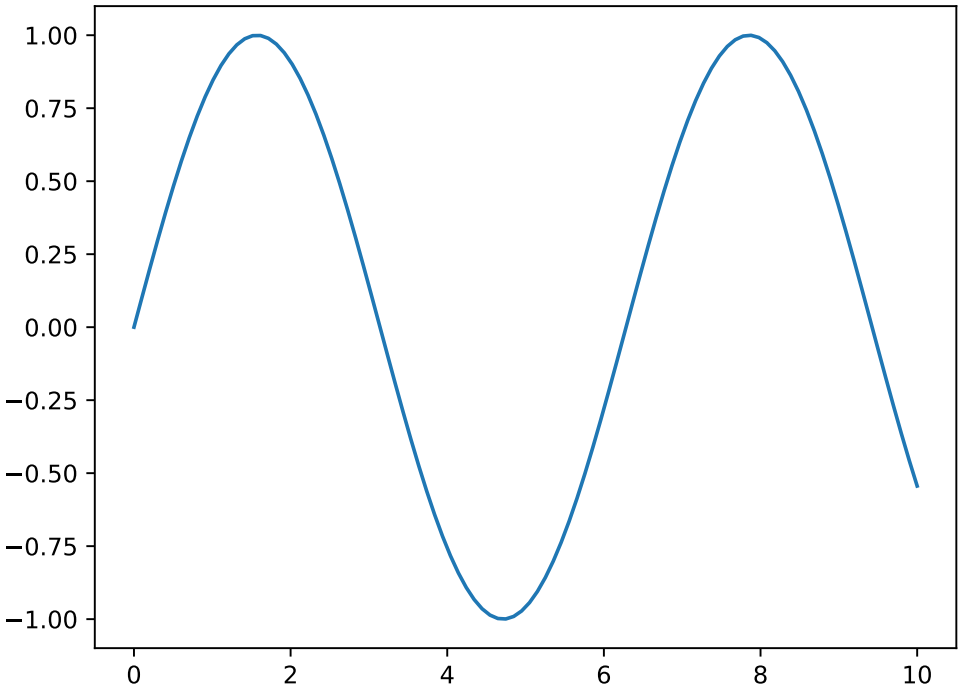
1.00
0.75
0.50
0.25
0.00
−0.25
−0.50
−0.75
−1.00
0
2
4
6
8
10

# Part I

# Cosmological Structure Formation

# Chapter 2

# Preliminaries

## 2.1 General Relativity

### 2.1.1 Einstein's Field Equations

$$G_{\mu\nu} = 8\pi G T_{\mu\nu} \tag{2.1}$$

$$G_{\mu\nu} = R_{\mu\nu} - \frac{1}{2} g_{\mu\nu} R \tag{2.2}$$

$$R = g^{\mu\nu} R_{\mu\nu} \tag{2.3}$$

$$R_{\mu\nu} = \partial_\rho \Gamma^\rho_{\mu\nu} - \partial_\nu \Gamma^\rho_{\mu\rho} + \Gamma^\rho_{\mu\nu} \Gamma^\sigma_{\rho\sigma} - \Gamma^\rho_{\mu\sigma} \Gamma^\sigma_{\nu\rho} \tag{2.4}$$

### 2.1.2 Riemann Connection and Covariant Derivatives

$$\Gamma^\rho_{\mu\nu} = \frac{1}{2} g^{\rho\sigma} \left( \partial_\mu g_{\nu\sigma} + \partial_\nu g_{\mu\sigma} - \partial_\sigma g_{\mu\nu} \right) \tag{2.5}$$

$$\nabla_\mu T^\mu_\nu = \partial_\mu T^\mu_\nu + \Gamma^\mu_{\mu\alpha} T^\alpha_\nu - \Gamma^\alpha_{\mu\nu} T^\mu_\alpha \tag{2.6}$$

### 2.1.3 Geodesic Equation

$$\frac{d^2 x^\mu}{d\tau^2} + \Gamma^\mu_{\alpha\beta} \frac{dx^\alpha}{d\tau} \frac{dx^\beta}{d\tau} = 0 \tag{2.7}$$

### 2.1.4 The Stress-Energy Tensor

$$T_{\mu\nu} = (\rho + p) u_\mu u_\nu + p g_{\mu\nu} \tag{2.8}$$

## 2.2 Useful Relations

# Chapter 3

# Background Cosmology

## 3.1 The homogeneous Universe

In this chapter I will focus on explaining the background cosmology in light of a homogeneous universe. A natural place to start is the cosmological principle, followed by a description of the geometry of space itself. If not otherwise stated, the development of this chapter is based on Dodelson and F. Schmidt 2020, Weinberg 2008 and TODO: cite Baumann

### 3.1.1 The Cosmological Principle

### 3.1.2 The Robertson-Walker Metric

$$ds^2 = -dt^2 + a^2(t)\left[\frac{dr^2}{1-kr^2} + r^2 d\Omega^2\right] \tag{3.1}$$

### 3.1.3 The Friedmann Equations

## 3.2 My Universe is loaded with...

## 3.3 Thermal History of the Universe

# Chapter 4

# Perturbation Theory

## 4.1 Initial Conditions

## 4.2 Transfer Functions

## 4.3 Power Spectra

## 4.4 Linear Evolution

## 4.5 Non-linear Evolution

## 4.6 Bispectra

The bispectra are powerful tools for studying the non-linear evolution of the density field. The bispectrum is defined as the Fourier transform of the three-point correlation function, and is given by:

$$\langle \delta(\mathbf{k}_1)\delta(\mathbf{k}_2)\delta(\mathbf{k}_3)\rangle = (2\pi)^3\delta_D\left(\sum_i \mathbf{k}_i\right) B(\mathbf{k}_1,\mathbf{k}_2,\mathbf{k}_3) \tag{4.1}$$

### 4.6.1 Analytical Bispectum

$$B_\delta^{(3)}(\mathbf{k}_1,\mathbf{k}_2,\mathbf{k}_3) = 2\mathcal{P}_\delta(k_1)\mathcal{P}_\delta(k_2)F_2(\mathbf{k}_1,\mathbf{k}_2) + \text{cyc} \tag{4.2}$$

$$F_2(\mathbf{k}_1,\mathbf{k}_2) = \frac{5}{7} + \frac{x}{2}\left(\frac{k_1}{k_2}+\frac{k_2}{k_1}\right) + \frac{2}{7}x^2, \tag{4.3}$$

where $x = \hat{\mathbf{k}}_1\cdot\hat{\mathbf{k}}_2 = \cos\theta_{12}$, where $\theta_{12}$ is the angle spanned by $\mathbf{k}_1$ and $\mathbf{k}_2$. We could thus consequently write: $F_2(\mathbf{k}_1,\mathbf{k_2}) = F_2(k_1,k_2,\theta_{12})$ TODO: keep this here?

**Bispectrum of potential** Turn this into the bispectrum of the potential, and then use the Poisson equation to get the bispectrum of the density field. Start with the Poisson equation (at late times), valid for all scales as long as $\delta_\mathrm{m}$ is given in synchronous gauge:

$$\begin{aligned} k^2\Phi(\mathbf{k},a) &= 4\pi G a^2\rho_\mathrm{m}(a)\delta_\mathrm{m}(\mathbf{k},a) \\ \Phi(\mathbf{k},a) &= \frac{3}{2}\Omega_\mathrm{m}H_0^2\frac{\delta_\mathrm{m}(\mathbf{k},a)}{ak^2} \equiv \frac{\mathcal{C}(a)}{k^2}\delta_\mathrm{m}(\mathbf{k},a) \end{aligned} \tag{4.4}$$

where in the last step I used that $\rho_{\rm m}(a) = \Omega_{\rm m}\rho_{\rm crit}a^{-3}$ and $8\pi G\rho_{\rm crit} = 3H_0^2$. I also defined $\mathcal{C}(a) \equiv 3\Omega_{\rm m}H_0^2/(2a)$.

$$\begin{aligned}
\langle\Phi(\mathbf{k}_1,a)\Phi(\mathbf{k}_2,a)\Phi(\mathbf{k}_3,a)\rangle &= \frac{\mathcal{C}(a)^3}{k_1^2k_2^2k_3^2}\langle\delta_{\rm m}(\mathbf{k}_1,a)\delta_{\rm m}(\mathbf{k}_2,a)\delta_{\rm m}(\mathbf{k}_3,a)\rangle \\
(2\pi)^3\delta_D\left(\sum_i \mathbf{k}_i\right)B_\Phi(\mathbf{k}_1,\mathbf{k}_2,\mathbf{k}_3) &= \frac{\mathcal{C}(a)^3}{k_1^2k_2^2k_3^2}(2\pi)^3\delta_D\left(\sum_i \mathbf{k}_i\right)B_\delta(\mathbf{k}_1,\mathbf{k}_2,\mathbf{k}_3) \\
B_\Phi(\mathbf{k}_1,\mathbf{k}_2,\mathbf{k}_3) &= \frac{\mathcal{C}(a)^3}{k_1^2k_2^2k_3^2}B_\delta(\mathbf{k}_1,\mathbf{k}_2,\mathbf{k}_3)
\end{aligned} \tag{4.5}$$

TODO: fix some stuff with $a$ above Which leads to:

$$B_\Phi^{(3)}(\mathbf{k}_1,\mathbf{k}_2,\mathbf{k}_3) = \frac{\mathcal{C}(a)^3}{k_1^2k_2^2k_3^2}\left[2\mathcal{P}_\delta(k_1)\mathcal{P}_\delta(k_2)F_2(\mathbf{k}_1,\mathbf{k}_2) + \text{cyc}\right] \tag{4.6}$$

Using the same logic I find a relation between the power spectrum of the gravitational potential and the matter contrast:

$$\mathcal{P}_\Phi(k,a) = \frac{\mathcal{C}(a)^2}{k^4}\mathcal{P}_\delta(k,a) \Longleftrightarrow \mathcal{P}_\delta(k,a) = \frac{k^4}{\mathcal{C}(a)^2}\mathcal{P}_\Phi(k,a) \tag{4.7}$$

enables me to write:

$$\mathcal{P}_\delta(k_1)\mathcal{P}_\delta(k_2) = \frac{k_1^4k_2^4}{\mathcal{C}(a)^4}\mathcal{P}_\Phi(k_1)\mathcal{P}_\Phi(k_2) \tag{4.8}$$

This again leads to the following:

$$B_\Phi^{(3)}(\mathbf{k}_1,\mathbf{k}_2,\mathbf{k}_3) = \frac{\mathcal{C}(a)^{-1}}{k_1^2k_2^2k_3^2}\left[2\mathcal{P}_\Phi(k_1)\mathcal{P}_\Phi(k_2)\tilde{F}_2(\mathbf{k}_1,\mathbf{k}_2) + \text{cyc}\right] \tag{4.9}$$

where the modified $F_2$-kerner is given by:

$$\tilde{F}_2(\mathbf{k}_1,\mathbf{k}_2) \equiv k_1^4k_2^4\left[\frac{5}{7} + \frac{x}{2}\left(\frac{k_1}{k_2}+\frac{k_2}{k_1}\right) + \frac{2}{7}x^2 + \frac{2}{7}x^2\right] \tag{4.10}$$

# Chapter 5

# Simulation theory

Some theory and history as to how to conduct N-body simulations.

## 5.1 N-body simulations

### 5.1.1 Describing a box of particles

### 5.1.2 Forces and Fields

### 5.1.3 Mass Assignment Schemes

### 5.1.4 Validity of Box

## 5.2 Newtonian Approach

## 5.3 General Relativistic Approach

# Part II

# Machine Learning

# Chapter 6

# Fundamental Elements of Machine Learning

## 6.1 Introduction

In this chapter I will give a brief introduction into machine learning. This includes a mathematical description of some fundamental concepts common across numerous machine learning models. The more advanced models will be dealt with at a later stage. If not otherwise stated, the following chapter is based on Goodfellow, Bengio and Courville 2016 and Hastie, Tibshirani and Friedman 2009.

## 6.2 Linear Algebra

maybe

## 6.3 Probability and Information Theory

maybe

## 6.4 Basic Machine Learning

TODO: Fill more here

### 6.4.1 Estimators, Bias, Variance and Error

**Estimators** Based on the assumption that there exists some true parameter(s) $\boldsymbol{\theta}$ which remain unknown,[1] we are able to make predictions and estimations of such parameter(s). Let's say we have $m$ independent and identically distributed (i.i.d.) random variables $\{\mathbf{x}_1, \mathbf{x}_2, \ldots, \mathbf{x}_m\}$ drawn from the same probability distribution $p(\mathbf{x})$. An *estimator* of the true values $\boldsymbol{\theta}$ is any function of the data such that $\hat{\boldsymbol{\theta}}_m = g(\mathbf{x}_1, \ldots, \mathbf{x}_m)$, where $\hat{\boldsymbol{\theta}}$ is the estimate of $\boldsymbol{\theta}$. This is known as point estimation, as we are estimating a single value. This definition does not pose any restrictions on the function $g$. However, a good estimator would yield an estimate $\hat{\boldsymbol{\theta}}_m$ that is close to the true value $\boldsymbol{\theta}$.

[1] This is the frequentist perspective of statistics

**Function estimators** Say we want to predict a variable $\mathbf{y}$ given some vector $\mathbf{x}$. We assume the true variable $\mathbf{y}$ is given by some function approxiamation $f(\mathbf{x})$ plus some error $\boldsymbol{\epsilon}$: $\mathbf{y} = f(\mathbf{x}) + \boldsymbol{\epsilon}$. The aim is then to estimate the function $f$ with the estimator $\hat{f}$. If we then realise that $\hat{f}$ is really just a point estimator in function space, the two above concepts are equivalent.

**Bias** The bias of the estimator $\hat{\boldsymbol{\theta}}_m$ is defined as the difference between the expected value of the estimator and the true value of the parameter: $\text{bias}(\hat{\boldsymbol{\theta}}_m) = \mathbb{E}[\hat{\boldsymbol{\theta}}_m] - \boldsymbol{\theta}$. An unbiased estimator has zero bias, i.e. $\mathbb{E}[\hat{\boldsymbol{\theta}}_m] = \boldsymbol{\theta}$. An estimator is asymptotically unbiased if its bias approaches zero as the number of data points $m$ approaches infinity, i.e. $\lim_{m\to\infty} \mathbb{E}[\hat{\boldsymbol{\theta}}_m] = \boldsymbol{\theta}$.

#### Variance

#### Standard Error

#### Mean Squared Error

### 6.4.2 Maximum Likelihood Estimation

### 6.4.3 Bayesian Statistics

### 6.4.4 Supervised Learning

### 6.4.5 Unsupervised Learning

# Chapter 7

# Neural Networks

## 7.1 Forward pass - Prediction

### 7.1.1 Activation functions

### 7.1.2 Loss functions

## 7.2 Backpropagation - Training

### 7.2.1 Gradient descent

### 7.2.2 Optimizers

### 7.2.3 Regularization

# Chapter 8

# Convolutional Neural Networks

## 8.1 Convolution

## 8.2 New Layers

### 8.2.1 Convolutional layers

### 8.2.2 Pooling layers

### 8.2.3 Dropout layers

# Part III

# Acquiring Data

# Chapter 9

# Simulations

## 9.1 Parameters

When performing simulations, it was import to keep all parameters fixed for all the different simulations. The only thing that was changed was the random seed.

### 9.1.1 Cosmological parameters

The relevant cosmological parameters are the dimensionless Hubble factor $h$, the baryon and cold dark matter densities $\Omega_b$ and $\Omega_{\mathrm{CDM}}$, the Cosmic Microwave Background temperature $T_{\mathrm{CMB}}$ and the effective number of ultra-relativistic neutrinos $N_{\mathrm{ur}}$.

Table 9.1: Cosmological parameters

| Parameter | Value | Unit |
|---|---|---|
| $h$ | 0.67556 | - |
| $\Omega_b$ | 0.022032 | - |
| $\Omega_{\mathrm{CDM}}$ | 0.12038 | - |
| $T_{\mathrm{CMB}}$ | 2.7255 | K |
| $N_{\mathrm{ur}}$ | 3.046 | - |

### 9.1.2 Primordial power spectrum

The primordial power spectrum, as TODO: link to when written,contains the pivot scale $k_{\mathrm{piv}}$, the primordial amplitude, $\mathcal{A}_{\mathrm{s}}$ and the spectral index, $n_{\mathrm{s}}$.

Table 9.2: Primordial power spectra parameters

| Parameter | Value | Unit |
|---|---|---|
| $k_{\mathrm{piv}}$ | 0.05 | $\mathrm{Mpc}^{-1}$ |
| $\mathcal{A}_{\mathrm{s}}$ | $2.215 \cdot 10^{-9}$ | - |
| $n_{\mathrm{s}}$ | 0.9619 | - |

### 9.1.3 Box parameters

The relevant box parameters were the initial redshift $z_{\text{ini}}$ where the simulations were started from. The simulations box itself was characterised by the physical length $L$, represented on a cube grid of size $N_{\text{grid}}^3$, resulting in a resolution of $\Delta_{\text{res}} = L/N_{\text{grid}}$. The courant factor TODO: fill and time step limit TODO: fill. This resulted in a fundamental

Table 9.3: Box parameters

| Parameter | Value | Unit |
|---|---|---|
| $z_{\text{ini}}$ | 100 | |
| $L$ | 5120 | Mpc |
| $N_{\text{grid}}$ | 256 | px |
| $\Delta_{\text{res}}$ | $20 (= L/N_{\text{grid}})$ | Mpc px$^{-1}$ |
| Courant factor | 48 | ? |
| Time step limit | 0.04 | ? |

frequency of $k_{\text{F}} = 2\pi/L$ and Nyquist freguency $k_{\text{N}} = \pi/\Delta_{\text{res}}$ TODO: what with units?

### 9.1.4 Seeds

In order to initialise the simulations we used random seeds, one for each simulation. This ensured that analysis performed on different simulations were of different realisations of the simulated universe, essential statistical independence. The seeds, denoted as $\mathtt{S}$ ranged from 0 to 2000, and consisted of the following set:

$$\{\mathtt{S} \in \mathbb{Z} | 0 \leq \mathtt{S} < 2000\} \tag{9.1}$$

### 9.1.5 Output

$$z_{\text{d}} = \{20, 15, 10, 5, 1, 0\} \tag{9.2}$$

$$z_{\text{p}} = \{100, 50, 20, 15, 10, 6, 5, 4, 3, 2, 1, 0.9, 0.8, 0.7, 0.6, 0.5, 0.4, 0.3, 0.2, 0.1, 0\} \tag{9.3}$$

$$\mathcal{D}(\mathtt{S}, z_{\text{d}}) \tag{9.4}$$

$$\mathcal{D}_{\Phi}(\mathtt{S}, z_{\text{p}}) \tag{9.5}$$

$$\mathcal{D}_{\delta}(\mathtt{S}, z_{\text{p}}) \tag{9.6}$$

# Chapter 10

# Data Verification

## 10.1 Slices of Datacubes

## 10.2 Powerspectra from Simulations

## 10.3 Powerspectra from Datacubes

## 10.4 Analytical Bispectra

$$B^{(3)}(k_1, k_2, k_3) = 2\mathcal{P}(k_1)\mathcal{P}(k_2)F_2(\mathbf{k}_1, \mathbf{k}_2) + \text{cyc} \tag{10.1}$$

$$F_2(\mathbf{k}_1, \mathbf{k}_2) = \frac{5}{7} + \frac{x}{2}\left(\frac{k_1}{k_2} + \frac{k_2}{k_1}\right) + \frac{2}{7}x^2, \tag{10.2}$$

where $x = \hat{\mathbf{k}}_1 \cdot \hat{\mathbf{k}}_2 = \cos\theta_{12}$, where $\theta_{12}$ is the angle spanned by $\mathbf{k}_1$ and $\mathbf{k}_2$. We could thus consequently write: $F_2(\mathbf{k}_1, \mathbf{k_2}) = F_2(k_1, k_2, \theta_{12})$

Given $k_1$ and $k_2$ and $\theta_{12}$ we have the following relations, with reference to Section 10.4:

$$\begin{aligned} \alpha &= \pi - \theta_{12} \\ \beta &= \pi - \theta_{23} \\ \gamma &= \pi - \theta_{31} \end{aligned} \tag{10.3}$$

From cosine rule:

$$k_3 = \sqrt{k_1^2 + k_2^2 - 2k_1k_2\cos\alpha} \tag{10.4}$$

From the rule of sines TODO: explain more?:

$$\begin{aligned} \beta &= \arcsin\left(\frac{k_1}{k_3}\sin\alpha\right) \\ \gamma &= \arcsin\left(\frac{k_2}{k_3}\sin\alpha\right) \end{aligned} \tag{10.5}$$

## 10.5 Bispectra from Cube

### 10.5.1 Binning

### 10.5.2 Bispectra

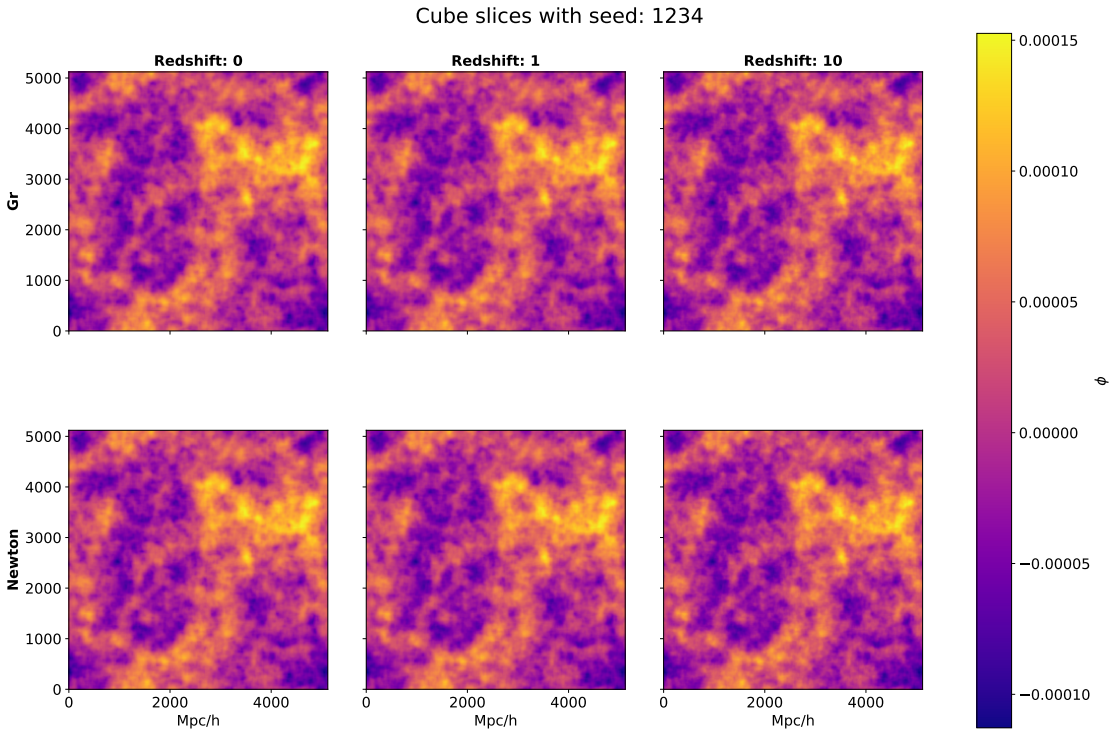


Figure 10.1: Slice 0

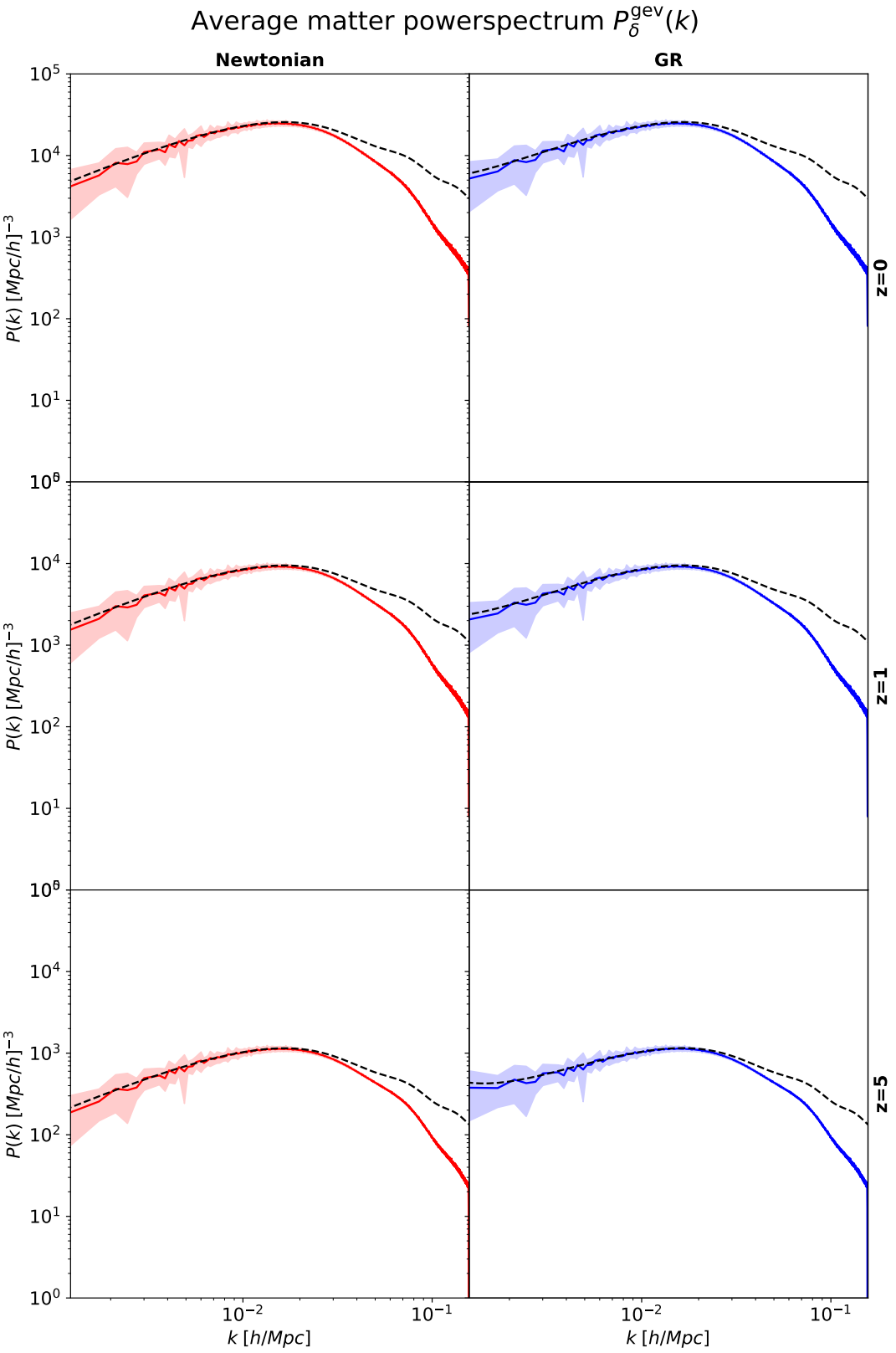


Figure 10.2: Average matter power spectra at different redshifts.

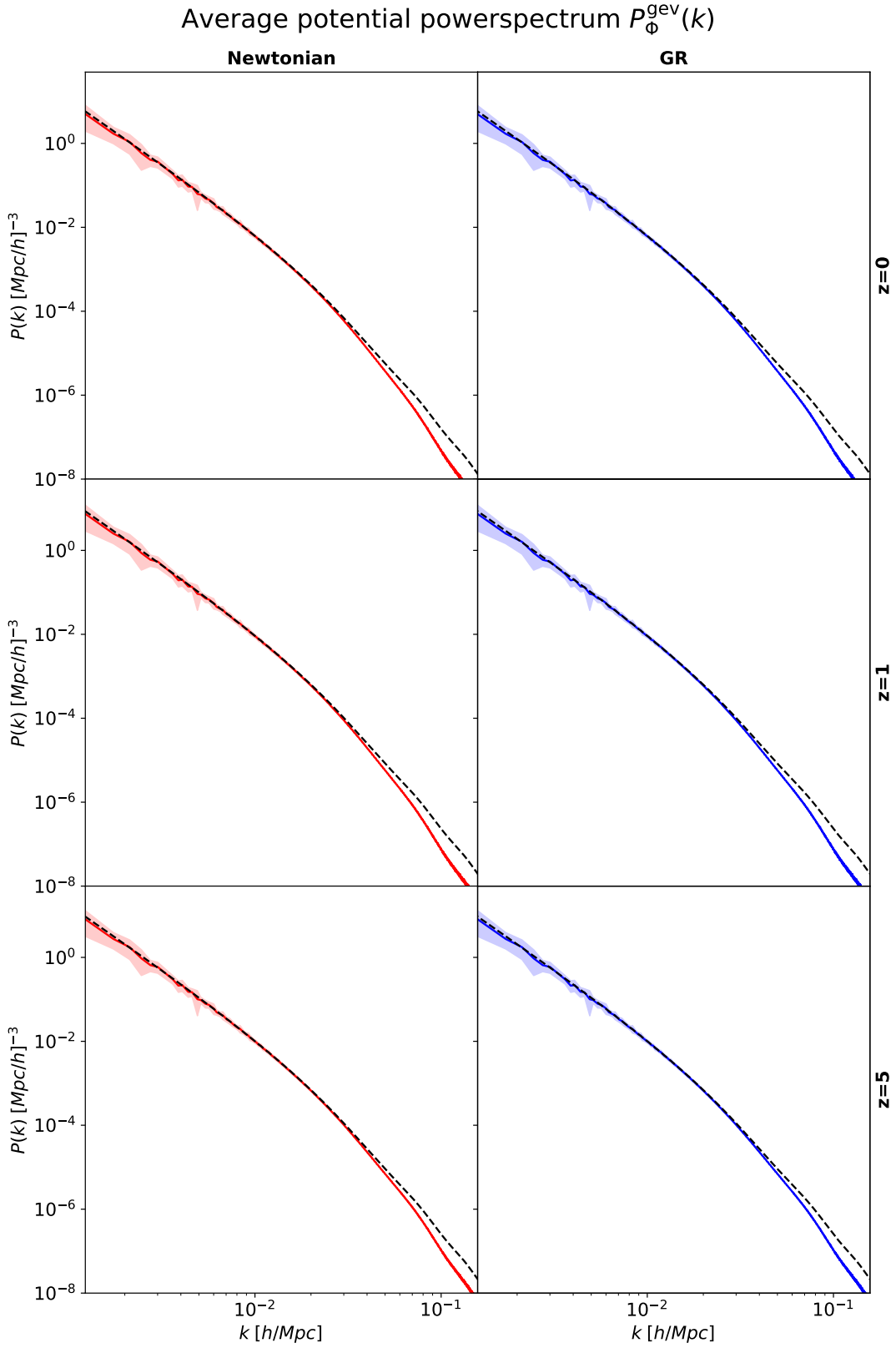


Figure 10.3: Average potential power spectra at different redshifts.

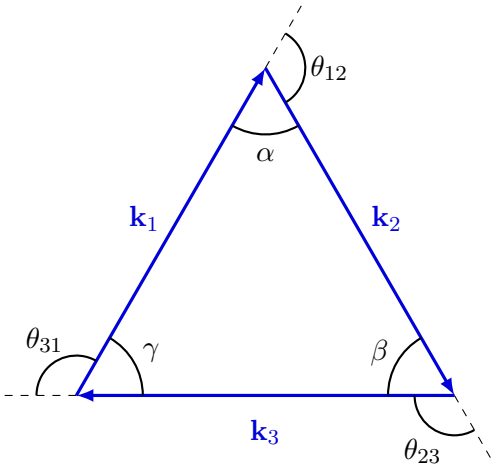


Figure 10.4: Angles in arbitrary bispectrum triangle configuration.

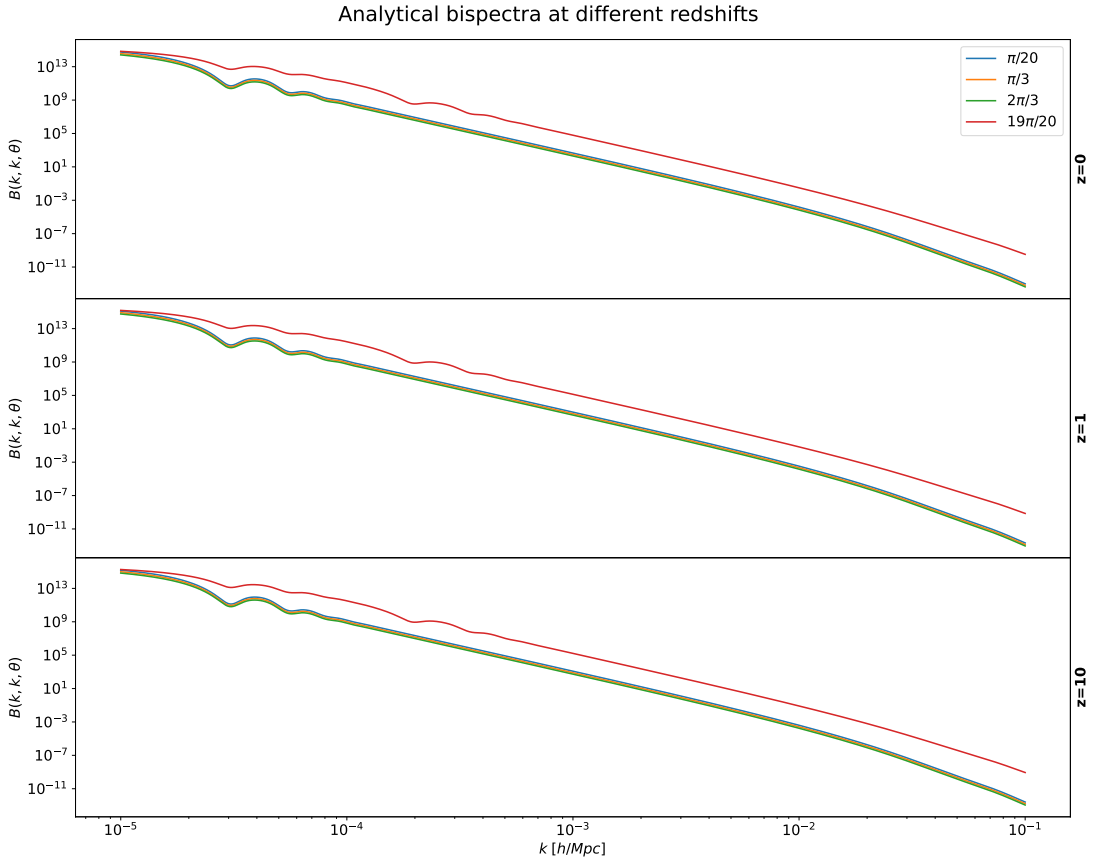

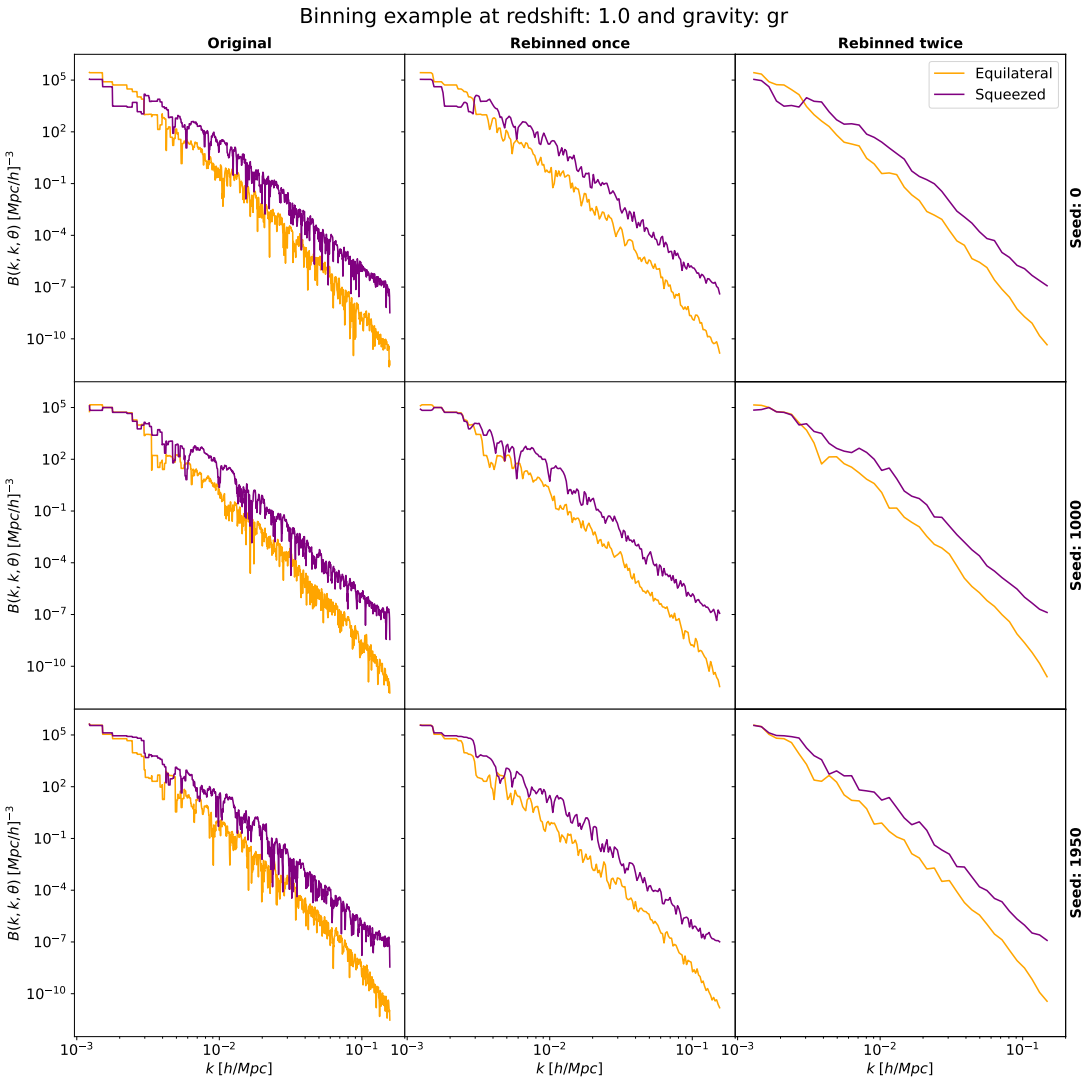
Binning example at redshift: 1.0 and gravity: gr
Original
Rebinned once
Rebinned twice
Equilateral
Squeezed
Seed: 0
Seed: 1000
Seed: 1950
$B(k,k,\theta)$ $[Mpc/h]^{-3}$
$k$ $[h/Mpc]$

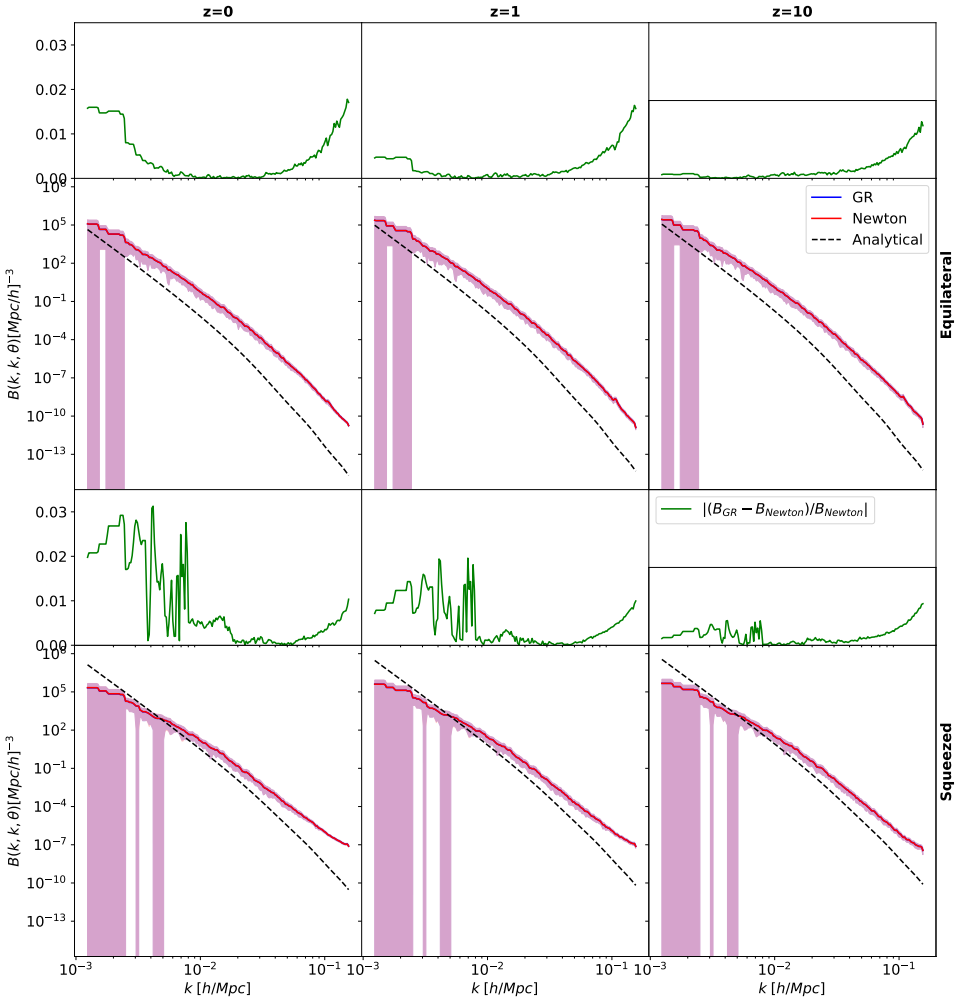
z=0
z=1
z=10
GR
Newton
Analytical
$|(B_{GR} - B_{Newton})/B_{Newton}|$
Equilateral
Squeezed
$B(k, k, \theta)[Mpc/h]^{-3}$
$k$ [$h$/Mpc]

# Chapter 11

# Trainable Dataset

# Bibliography


Adamek, Julian et al. (29th July 2016). 'gevolution: a cosmological N-body code based on General Relativity'. In: *Journal of Cosmology and Astroparticle Physics* 2016.7, pp. 053–053. ISSN: 1475-7516. DOI: 10.1088/1475-7516/2016/07/053. arXiv: 1604.06065[astro-ph,physics:gr-qc,physics:physics]. URL: http://arxiv.org/abs/1604.06065 (visited on 23/08/2023).

Alqaraawi, Ahmed et al. (3rd Feb. 2020). *Evaluating Saliency Map Explanations for Convolutional Neural Networks: A User Study*. arXiv: 2002.00772[cs]. URL: http://arxiv.org/abs/2002.00772 (visited on 23/10/2023).

Chisari, Nora Elisa and Matias Zaldarriaga (2nd June 2011). 'Connection between Newtonian simulations and general relativity'. In: *Physical Review D* 83.12, p. 123505. ISSN: 1550-7998, 1550-2368. DOI: 10.1103/PhysRevD.83.123505. arXiv: 1101.3555[astro-ph,physics:gr-qc]. URL: http://arxiv.org/abs/1101.3555 (visited on 23/08/2023).

Dodelson, S. and F. Schmidt (2020). *Modern Cosmology*. Elsevier Science. ISBN: 9780128159484. URL: https://books.google.no/books?id=GGjfywEACAAJ.

Goodfellow, Ian, Yoshua Bengio and Aaron Courville (2016). *Deep Learning*. http://www.deeplearningbook.org. MIT Press.

Green, Stephen R. and Robert M. Wald (15th Mar. 2012). 'Newtonian and Relativistic Cosmologies'. In: *Physical Review D* 85.6, p. 063512. ISSN: 1550-7998, 1550-2368. DOI: 10.1103/PhysRevD.85.063512. arXiv: 1111.2997[astro-ph,physics:gr-qc]. URL: http://arxiv.org/abs/1111.2997 (visited on 23/08/2023).

Hastie, T., R. Tibshirani and J.H. Friedman (2009). *The Elements of Statistical Learning: Data Mining, Inference, and Prediction*. Springer series in statistics. Springer. ISBN: 9780387848846. URL: https://books.google.no/books?id=eBSgoAEACAAJ.

Jeong, Donghui, Fabian Schmidt and Christopher M. Hirata (4th Jan. 2012). 'Large-scale clustering of galaxies in general relativity'. In: *Physical Review D* 85.2, p. 023504. ISSN: 1550-7998, 1550-2368. DOI: 10.1103/PhysRevD.85.023504. arXiv: 1107.5427[astro-ph]. URL: http://arxiv.org/abs/1107.5427 (visited on 23/08/2023).

Selvaraju, Ramprasaath R. et al. (Feb. 2020). 'Grad-CAM: Visual Explanations from Deep Networks via Gradient-based Localization'. In: *International Journal of Computer Vision* 128.2, pp. 336–359. ISSN: 0920-5691, 1573-1405. DOI: 10.1007/s11263-019-01228-7. arXiv: 1610.02391[cs]. URL: http://arxiv.org/abs/1610.02391 (visited on 23/10/2023).

Weinberg, S. (2008). *Cosmology*. Cosmology. OUP Oxford. ISBN: 9780191523601. URL: https://books.google.no/books?id=nqQZdg020fsC.